


Observation of anomalous heat transport in a trapped ion chainZ.-C. Mao¹,* Y.-Z. Xu,^{*} Q.-X. Mei¹, W.-D. Zhao, Y. Jiang, Z.-J. Cheng, X.-Y. Chang, L. He, L. Yao, Z.-C. Zhou,[†] Y.-K. Wu,[‡] and L.-M. Duan[§]*Center for Quantum Information, Institute for Interdisciplinary Information Sciences, Tsinghua University, Beijing 100084, People's Republic of China* (Received 10 December 2021; revised 23 February 2022; accepted 28 February 2022; published 15 March 2022)

Energy transport in low-dimensional systems or systems with long-range interactions shows unusual properties not observed in conventional three-dimensional materials. Trapped linear ion chains have been proposed as an ideal platform to study such phenomena, but many predicted features have not been demonstrated yet and the existing experiments mainly focus on the weak excitation limit where the dynamics can be described by linearized phonon modes. Here, we study the energy transport in a chain of $^{174}\text{Yb}^+$ ions using a focused heating laser beam. Nontrivial effects are observed such as a nonmonotonic energy distribution with reflection symmetry, oscillatory heating dynamics, and a change in the heating pattern due to the competition between the external driving and interion coupling. Our work deepens the understanding about transport in low-dimensional systems and also provides guidelines for the sympathetic cooling of long ion chains, with applications in quantum information processing and precision measurement.

DOI: [10.1103/PhysRevA.105.033107](https://doi.org/10.1103/PhysRevA.105.033107)**I. INTRODUCTION**

Transport phenomena are one of the most important topics in condensed matter physics [1,2]. In normal three-dimensional (3D) materials, transport often takes a diffusive behavior where the transport rate is proportional to the gradient of a relevant quantity. Examples include the Fick's law for the diffusion of mass, Ohm's law for electrical transport, and Fourier's law for heat conduction [3]. Although such diffusion processes are relatively well understood for ordinary materials, in lower-dimensional [4,5] and long-range interacting [6] systems, exotic phenomena such as a divergent thermal conductivity in the thermodynamic limit have been predicted, which remain a hot spot of current research.

As the experimental technology develops, the ion trap has become an ideal platform to simulate the classical and quantum properties of many-body physics [7] owing to its strong stability [8] and controllability [9,10] as well as convenient initialization and readout [10]. Equipped with a natural long-range Coulomb interaction and available low-dimensional Wigner crystal structures [11,12], it has been widely applied to study the properties of unconventional materials such as structural phase transitions [13–21] and nanofrictions [22–24]. Extensive theoretical work has been conducted to understand the energy transport in one-dimensional (1D) or quasi-1D ion crystals [6,25–28] and counterintuitive phenomena such as a diverging conductivity with system sizes [27], the absence of a linear temperature gradient [6,27] or even a nonmonotonic temperature distribution [25], and nontrivial

dependence on the dissipation rate due to the competition with interion coupling [25]. Recently, the propagation of a single phonon on a 1D ion chain has been observed in experiments [29,30], as well as that of weak coherent excitations [31]. However, these experiments are all in the linear regime where the phonon dynamics are well described by collective normal modes. The possible role of nonlinearity due to the large amplitudes of ions in the heat propagation process remains unexplored. In addition, many intriguing properties, such as nonmonotonic local temperatures and the nontrivial dependence on the dissipation rate, have yet to be demonstrated in experiments.

In this paper, we study the anomalous heat propagation in a 1D Wigner crystal with a long-range interaction using trapped ions with a local heating laser beam. We demonstrate that, under suitable heating parameters, the energy distribution over the 1D chain is not monotonic and further exhibits a reflection symmetry. Also, we observe oscillatory behavior in the local temperature between two adjacent sites during the heating, which indicates an interference between the forward and backward propagations. Moreover, a nontrivial dependence of the temperature distribution on the external heating rate is observed. All of these are starkly different from conventional 3D materials and showcase the exotic properties in low-dimensional systems with long-range interactions. Apart from the fundamental scientific interest, our work also helps to understand sympathetic cooling in long ion chains [32–34] which finds wide applications in quantum information processing [35,36] and precision measurement [35,37,38].

II. SETUP

Our experimental setup and the pulse sequence are sketched in Fig. 1. We use a four-rod Paul trap to confine up to 20 $^{174}\text{Yb}^+$ ions along the axial z direction, with a radial trap

*These authors contributed equally to this work.

[†]zichaozhou@mail.tsinghua.edu.cn[‡]wyukai@mail.tsinghua.edu.cn[§]lmduan@tsinghua.edu.cn

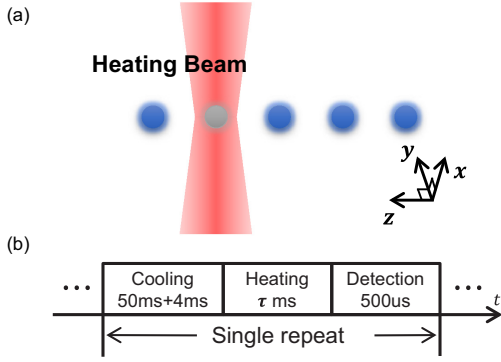


FIG. 1. (a) Schematic of the experimental setup. A linear chain of up to 20 $^{174}\text{Yb}^+$ ions are confined in a four-rod Paul trap. We apply a narrow heating laser beam along the transverse direction (at an angle of 45° with both the x and y principal axes) to provide a local heat source for the ion chain. With the help of global cooling or detection beams (not shown), the motion of the ions can be initialized or read out. (b) Experimental sequence. A two-stage Doppler cooling process, which consists of a 50-ms strong laser beam with far red detuning followed by a 4-ms weaker laser beam with smaller detuning, initializes the ions to the Doppler cooling limit. Then the local heating beam is applied on the target ion for a varied duration τ , after which the fluorescence of individual ions under the global detection beam is collected by a CCD camera. This process is repeated for 800 times and the images are added up to fit the ions' amplitudes.

frequency $\omega_r \approx 2\pi \times 1.02$ MHz and an axial trap frequency between $\omega_z = 2\pi \times 79.4$ and $2\pi \times 31$ kHz. A narrow laser beam with a waist radius of $6.7 \mu\text{m}$, which is smaller than the ion spacing around $10 \mu\text{m}$, can be applied on any target ion to provide local heating. Before each experiment, we initialize the motional state of the ion chain by a two-stage global Doppler cooling: First, we apply a $29\text{-}\mu\text{W}$ strong cooling beam, corresponding to a saturation parameter $s \equiv I/I_s = 4.3$ [10], with detuning $\Delta = -2\pi \times 46$ MHz for 50 ms to cool down ions with high energy; then we reduce the laser power to $2 \mu\text{W}$, $s = 0.29$, and the detuning to $\Delta = -2\pi \times 10$ MHz for another 4 ms to approach the Doppler cooling limit. Then we turn on the heating beam at various locations for various durations to insert the energy into the system and let it propagate within the chain. In this experiment, we keep using 70-nW power for the blue-detuned heating laser, which corresponds to a saturation parameter $s \approx 2$, and tune the laser frequency to adjust the heating rate. Finally, a $500\text{-}\mu\text{s}$ global detection beam with $1\text{-}\mu\text{W}$ power and $\Delta = -2\pi \times 2$ MHz detuning is used to image all the ions. We repeat the experimental sequence for 800 times and add up the images together, from which the transverse amplitudes of individual ions can be fitted as an indicator of the local temperatures (see Appendix A for details). Unlike our previous works [34,39], here we focus on the transverse motion because of the slower energy propagation dynamics compatible with our measurement scheme, even though its amplitude is typically smaller than that for the axial motion.

We also perform numerical simulations for the ions' dynamics to compare with the experiments. During the heating process, the ions can acquire large amplitudes comparable to their distances, so that a linearized description based on

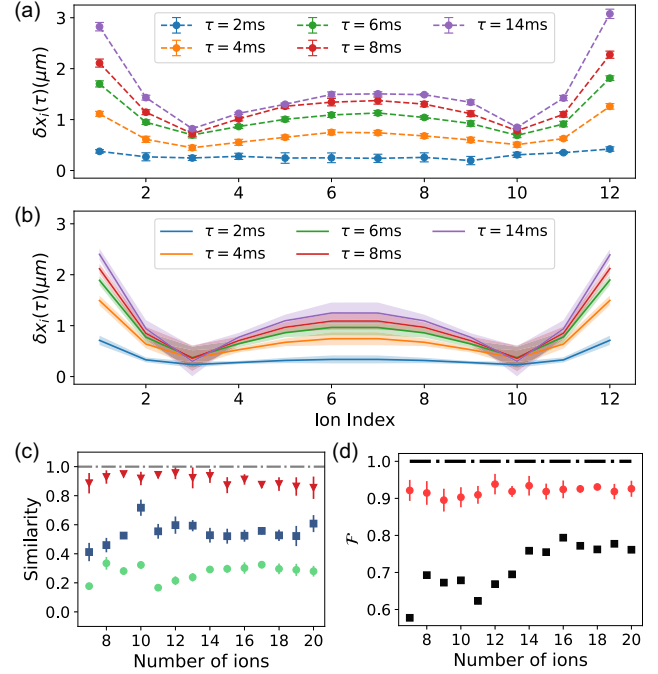


FIG. 2. (a) The measured amplitude δx_i of each ion in an $N = 12$ ion chain with the heating beam applied on the first ion on the left for various times τ . Data points are connected by dashed lines to guide the eyes. The amplitudes of all the ions are increasing with time, but the rates are nonuniform and show a reflection symmetry over the chain. (b) The corresponding theoretical results by simulating the dynamics of the ions starting from an initial temperature $T_0 = 4.5$ mK. For the heating laser beam we use a saturation parameter $s = 2$ and a blue detuning $\Delta = 2\pi \times 12$ MHz, with its finite width considered. To simulate the effect of $500\text{-}\mu\text{s}$ detection time in the experiment, here we also compute the average amplitude $\sqrt{\langle x_i^2(t) \rangle}$ for $500\text{-}\mu\text{s}$ duration. We further average the simulation for 100 random trials with the shaded region representing one standard deviation. (c) Similarity between the heated ion (the first ion on the left) and other ions for various ion numbers after $\tau = 10$ ms heating. Red triangles are for its symmetric partner (the first ion on the right), and the green circles and the blue squares are for the remaining ions with the minimal and the maximal energy, respectively. (d) The symmetry factor \mathcal{F} (red dots) for various ion numbers after heating the first ion on the left of the chain for $\tau = 10$ ms. For a perfect reflection symmetry we would get $\mathcal{F} = 1$ (dashed-dotted line). On the other hand, if ions are paired randomly rather than following the reflection symmetry, the computed symmetry factor would be the black squares, far below the symmetric case. Each measured amplitude is fitted as the Gaussian width of the image when adding up the photon counts for 800 repetitions. This sequence is further repeated ten times to estimate the standard deviation as the error bars.

the normal modes may not be valid. Therefore we perform molecular dynamics simulations for the ions with mass m and charge e under an external harmonic potential and the Coulomb interaction,

$$U = \sum_i \frac{1}{2} m (\omega_x^2 x_i^2 + \omega_y^2 y_i^2 + \omega_z^2 z_i^2) + \sum_{i < j} \frac{e^2}{4\pi\epsilon_0} \frac{1}{|\vec{r}_i - \vec{r}_j|}. \quad (1)$$

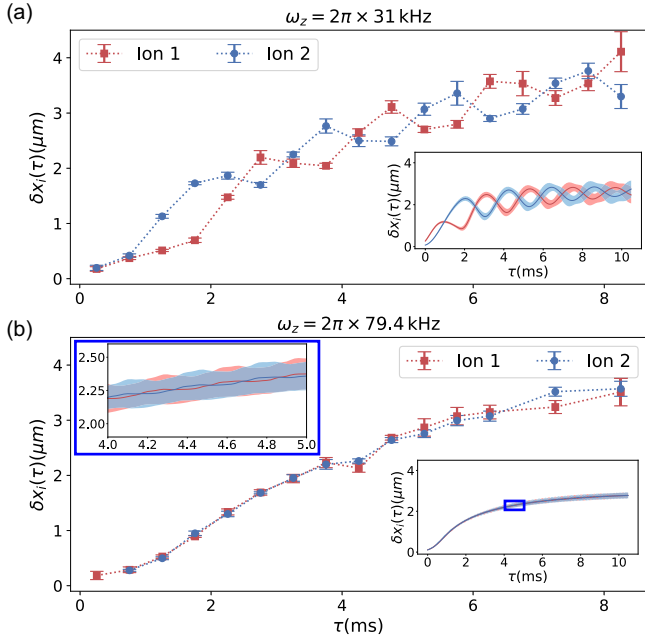


FIG. 3. Nonmonotonic heating dynamics in an $N = 2$ ion crystal. The heating beam is on ion 1 plotted in red and the other ion is plotted in blue. For (a) a low axial trap frequency $\omega_z = 2\pi \times 31$ kHz and thus large ion distance, apart from the global increase in the energy of the two ions, oscillatory behavior is observed as an indicator of the back-and-forth energy exchange. This is consistent with the theoretical simulation as shown in the inset. For (b) a higher axial trap frequency $\omega_z = 2\pi \times 79.4$ kHz and hence smaller ion distance, such oscillatory behavior is still predicted in theory (see the lower-right panel and a zoom-in for the region in its blue box on the upper left), but with a higher frequency and a lower amplitude, which makes it difficult to observe in the experiment. The measured data points are connected by dotted lines to guide the eyes. Error bars indicate one standard deviation estimated from five repetitions.

In addition, we model the effect of the heating beam as the random absorption and scattering of photons such that the momentum change of ion i in a short-time interval Δt is given by

$$m\Delta v_i^\xi = -\frac{\partial U}{\partial r_i^\xi} \Delta t + \sum_{j=1}^{N_p} \hbar(k^\xi - k_j'^\xi), \quad (2)$$

where $i = 1, \dots, N$ indicates each ion and $\xi = x, y, z$ for each spatial direction. The absorbed photon has a wave vector \vec{k} of the heating laser beam, and the scattered photon has a wave vector \vec{k}'_j with the same magnitude but in a random direction. The number of absorbed and scattered photons N_p follows a Poissonian distribution $N_p \sim \text{Pois}(\lambda = \Gamma \rho_{ee} \Delta t)$, where Γ is the natural linewidth of the atomic transition and $\rho_{ee}(\vec{v}_i) = (s/2)/[1 + s + 4(\Delta - \vec{k} \cdot \vec{v}_i)^2/\Gamma^2]$ the population on the excited state [10]. By introducing the position-dependent saturation parameter $s(\vec{r})$ with a Gaussian profile, we can take the effect of a finite laser beam width into account. If expanded to a linear term in velocity, this expression reduces to the commonly used one for the Doppler

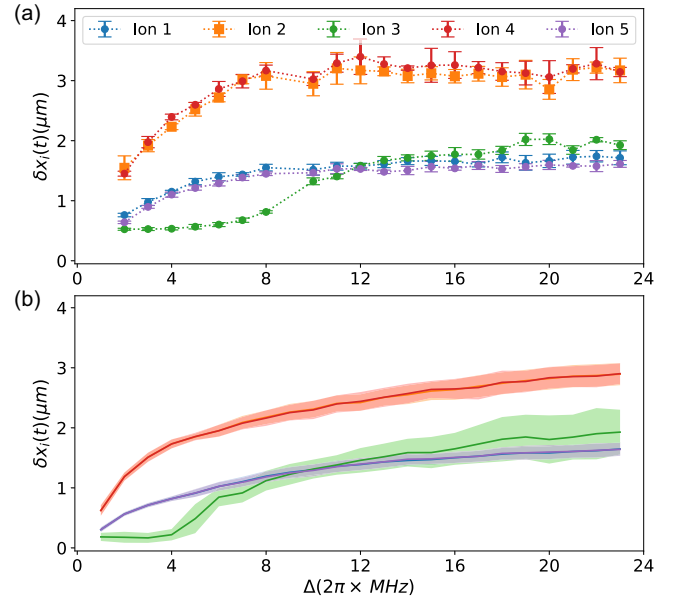


FIG. 4. Nontrivial energy propagation pattern vs the heating rate. (a) We adjust the heating rate by the blue detuning of the heating laser beam, which locates on the second ion in an $N = 5$ chain. While the amplitude of individual ions generally increases with the heating rate, the relative amplitudes of the central and the marginal ions reverse near $\Delta \approx 2\pi \times 12$ MHz, which arises from the competition between the driving and the propagation of energy on the chain. Here, we keep using a heating time $\tau = 10$ ms. (b) The numerical simulation results show a qualitative agreement with the experiment.

cooling [10] except that here we have a blue detuning rather than a red one.

III. ANOMALOUS ENERGY DISTRIBUTION

Equipped with these experimental and theoretical tools, now we can study the heat propagation dynamics. In Fig. 2, we fix the heating beam at the leftmost ion and its detuning to $\Delta = 2\pi \times 12$ MHz to study the energy distribution over the chain. As we can see in Fig. 2(a), while the local temperatures of all the ions (characterized by their transverse amplitudes) are consistently rising with the heating time, the increasing rates vary over the chain and the resulting energy distribution is neither uniform, nor does it possess a linear gradient. Instead, a spatial reflection symmetry over the chain can be observed for the energy distribution, and the rightmost ion, despite lacking a local heating source, demonstrates a higher local temperature than its neighbors while its energy is still increasing. This is a clear violation of the Fourier's law and is also confirmed by our numerical simulation under similar parameters as shown in Fig. 2(b). Actually, such a symmetric distribution has been predicted in the weak excitation limit [25] and observed during the melting process of an ion crystal for the axial motions [39]. Here, we perform a further quantitative analysis for this reflection symmetry.

Let us define the similarity between the local temperatures of ion i and ion j as $S_{ij} \equiv 1 - |\langle \delta x_i^2 \rangle - \langle \delta x_j^2 \rangle| / (\langle \delta x_i^2 \rangle + \langle \delta x_j^2 \rangle)$, which is a value between 0 and 1 with higher values indicating a stronger similarity between the two sites. In Fig. 2(c) we plot the similarity between the ion 1 (the leftmost

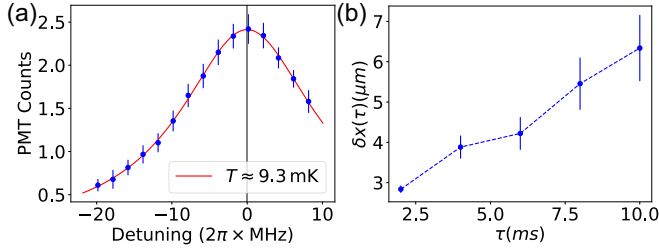


FIG. 5. (a) Fitting the fluorescence spectrum of a single ion after Doppler cooling by a Voigt line shape. We extract a temperature of about 9 mK. (b) The measured transverse amplitude vs the heating time. A positive correlation is observed, thus δx can be used to represent the local temperature.

ion being heated) and the ion N (red triangles, the symmetric partner), and that between the ion 1 and the ion with the lowest (green circles) and the highest (blue squares) local temperatures in the rest of the ions, in a chain with $N = 7-20$ after $\tau = 10$ ms heating. While the similarity between ion 1 and ion N stays high, there always exist low-energy ions with more than 50% differences, and even the hottest ion among 2 to $N-1$ has a significant difference from ion 1 and ion N . Furthermore, we define an overall symmetry factor $\mathcal{F} \equiv (1/[N/2]) \sum_i^{[N/2]} S_{i,N-i}$, which is the average similarity for all the symmetric pairs (for an odd number of ions we exclude the middle one). For an ion chain with perfect reflection symmetry, we would get $\mathcal{F} = 1$ as the black dashed-dotted line in Fig. 2(d). Our measured values for $N = 7-20$ when heating the leftmost ion for $\tau = 10$ ms are plotted as the red circles which are typically above 90%. In comparison, if we randomly pair different ions in the chain without respecting the reflection symmetry, the computed \mathcal{F} using the measured local δx_i would be the black squares, which are far below the red circles. This quantitatively confirms a nonuniform energy distribution together with a reflection symmetry over the chain.

IV. NONMONOTONIC HEATING DYNAMICS

In Fig. 2(a) it seems that the local temperature of each site is increasing monotonically with time. However, this can be due to the finite-time resolution in our experiment. In Fig. 3(a) we slow down the energy propagation by enlarging the ion spacing for a zoomed-in study of the heat propagation. For two ions at large distance, we observe clear oscillatory behavior in their local temperatures on top of a global heating process, which agrees well with our numerical simulation. A similar oscillation in local energy has also been reported in earlier works [31] in the weak excitation limit. In our case, although the nonlinear effect can already exist due to the large amplitudes, an analysis based on the collective modes can still provide a qualitative understanding. Specifically, the observed oscillation period of about 2 ms matches relatively well with the frequency difference $\Delta\omega = \omega_c - \omega_r = 2\pi \times 0.47$ kHz between the center-of-mass mode and the relative mode. Since in a long ion chain the collective modes can be expressed as plane waves [40], the nonmonotonic heating dynamics here can be explained as an interference between the forward propagations and the reflected ones. On the other

hand, when we increase the axial trapping frequency to reduce the ion spacing and thus speed up the energy transport, as illustrated in Fig. 3(b), the theoretical simulation predicts a much faster and weaker oscillation, which cannot be resolved in the experiment due to a detection time of 500 μs . A similar situation occurs if we increase the ion number (not shown) which again leads to a reduced ion spacing.

V. NONTRIVIAL DEPENDENCE ON EXTERNAL DRIVING

Finally, we examine the dependence of the energy transport on the external heating rate. In conventional materials, one would expect the system to respond linearly with the heating rate, but Ref. [25] shows that in 1D ion crystals there can be a nontrivial dependence due to the competition between the dissipation and the propagation effects. In Fig. 4, we tune the frequency of the heating beam to adjust its heating rate. In the linear regime, the heating rate can be expressed as $4s(\hbar k^2/m)(\Delta/\Gamma)/(1+s+4\Delta^2/\Gamma^2)^2$ [10] and is expected to increase with the detuning Δ from zero to $\sqrt{1+s}\Gamma/2 \approx 2\pi \times 17$ MHz for $s = 2$, while both in our experiment and in the numerical simulation, we observe that the temperature of the system is increasing when Δ is increased up to more than $2\pi \times 20$ MHz which is possibly due to the nonlinear effects. Although the amplitudes of individual ions (always measured for a fixed heating time of $\tau = 10$ ms) are consistently increasing with the heating rate (apart from possible experimental fluctuations), we also notice that the energy distribution pattern changes. In particular, by heating the second ion of an $N = 5$ chain, we observe that at a low driving rate (small detuning), the central ion has a much lower amplitude than the two ions on the edge, while as the driving rate goes up to some level, the central ion starts to heat up faster than the outer ones and finally its amplitude exceeds those of the outer ions after around $\Delta = 2\pi \times 12$ MHz. A similar phenomenon is also verified by our numerical simulation as shown in Fig. 4(b). This can be explained qualitatively as follows: The inner ions have smaller spacings than the outer ones so that the coupling to them is stronger; according to Ref. [25], the energy transport can be more efficient when the dissipation rate is comparable to the interior coupling; hence at a low heating rate, more energy goes to the outer ions, while at a high heating rate the energy prefers to go to the inner ion.

VI. CONCLUSION

To sum up, we have demonstrated and analyzed the nontrivial features of energy transport in a 1D system with long-range interactions that are distinctly different from conventional 3D materials. Nonmonotonic spatial and temporal behaviors are observed in the experiment and are confirmed by numerical simulation, and the reflection symmetry of the energy distribution is analyzed quantitatively. By tuning the external heating rate, we also showcase a change in the propagation pattern due to the competition between the dissipation and the coupling. Our work deepens the understanding about transport in low-dimensional systems and helps to design sympathetic cooling schemes for large 1D ion crystals that may be heated by local collisions with the background gases.

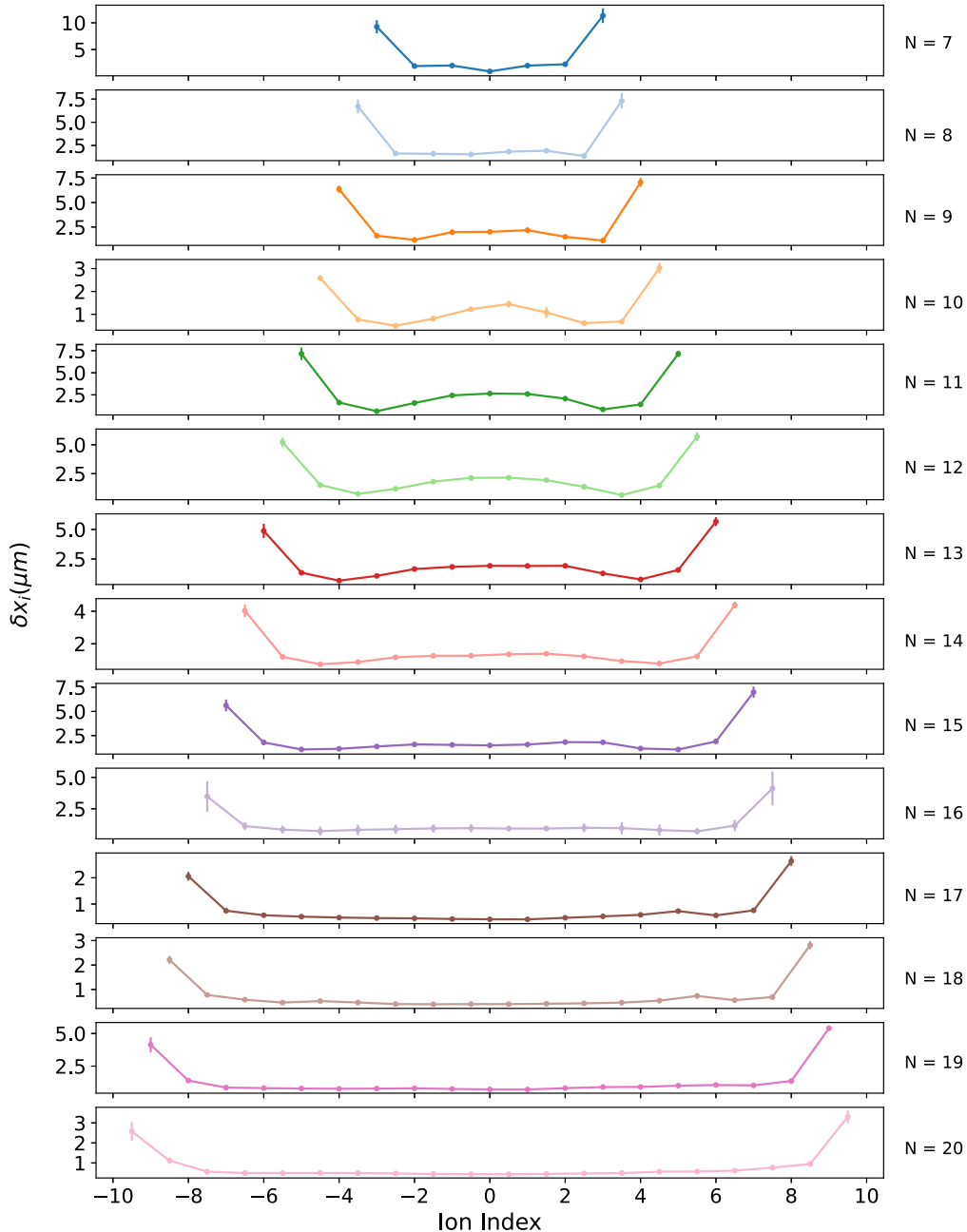


FIG. 6. Distribution of the transverse amplitudes δx_i at heating time $\tau = 10$ ms, similar to Fig. 2(a) of the main text. The ion indices are shifted to center at 0.

ACKNOWLEDGMENTS

This work was supported by the Frontier Science Center for Quantum Information of the Ministry of Education of China, and Tsinghua University Initiative Scientific Research Program. Y.-K.W. acknowledges support from the start-up fund from Tsinghua University.

APPENDIX A: MEASURING LOCAL TEMPERATURES BY TRANSVERSE AMPLITUDES

Following Ref. [25], we use the transverse amplitudes of the ions to represent their local temperatures. After obtaining

the image of each ion, we fit the radial profile by a Gaussian function and extract its standard deviation σ_G (in terms of the number of pixels) which satisfies [41]

$$\sigma_G^2 = \sigma_{\text{PSF}}^2 + M^2 \sigma_{\text{ion}}^2, \quad (\text{A1})$$

where M is the magnification of the imaging system, σ_{PSF} the width of the imaging point-spread function (PSF) caused by the diffraction of the system, and σ_{ion} the desired amplitude of the ions. In our system we find that one pixel of the CCD camera corresponds to about $0.43 \mu\text{m}$. Hence we have a magnification of $M \approx 2.33 \text{ pixels}/\mu\text{m}$.

In order to calibrate σ_{PSF} , we first cool an ion to the Doppler limit as described in the main text. We scan the detuning of the detection laser at a saturation parameter $s \approx 0.15$ and measure the fluorescence spectrum as shown in Fig. 5(a). Assuming the same temperature in the Doppler limit for the radial and the axial modes, which are both at an angle of 45° from the detection beam, we estimate the temperature of the ion as $T_D \approx 9$ mK by fitting a Voigt line shape [42] which is a convolution of Lorentzian and Gaussian functions. This gives us a theoretical rms spread in the transverse direction of about $\delta x_0 = 103$ nm under $\omega_r = 2\pi \times 1.02$ MHz [41]. By measuring the full width at half maximum (FWHM) of ions σ_{GC} after global Doppler cooling, we thus calibrate $\sigma_{\text{PSF}} = \sqrt{\sigma_{\text{GC}}^2 - M^2 \delta x_0^2}$. Combining σ_{PSF} , σ_{G} , and M , we can finally obtain σ_{ion} , which is used as the measured δx_i for individual ions. Actually, since δx_0 is much smaller than the diffraction limit σ_{PSF} , which in turn is much smaller than the later amplitudes after heating σ_{G} , a small error in calibrating T_D or δx_0 will not significantly affect the later results.

In the experiment, we notice that the image of an ion does not necessarily follow a Gaussian distribution, but as we demonstrate in Fig. 5(b), the extracted amplitude $\delta x(\tau)$ is positively correlated with the heating time τ , which in turn relates positively to the local temperature, when a heating beam is applied on an ion with a saturation parameter $s \approx 2$. Therefore, the transverse amplitude measured in this way can be a suitable indicator of the local temperature of the ion.

APPENDIX B: ADDITIONAL DATA FOR REFLECTION SYMMETRY IN HEAT PROPAGATION

In Fig. 6 we present similar plots as Fig. 2(a) in the main text at $\tau = 10$ ms for various ion numbers from $N = 7$ to 20, from which the data points in Figs. 2(c) and 2(d) can be computed. Although the detailed shape of the distribution varies with N , the nonmonotonic property and the reflection symmetry as described in the main text always exist in these figures.

-
- [1] C. Kittel, *Introduction to Solid State Physics*, 8th ed. (Wiley, Hoboken, NJ, 2004).
 - [2] M. P. Marder, *Condensed Matter Physics*, 2nd ed. (Wiley, Hoboken, NJ, 2011).
 - [3] J. L. Plawsky, *Transport Phenomena Fundamentals*, 4th ed. (CRC Press, London, 2020).
 - [4] S. Lepri, R. Livi, and A. Politi, Thermal conduction in classical low-dimensional lattices, *Phys. Rep.* **377**, 1 (2003).
 - [5] A. Dhar, Heat transport in low-dimensional systems, *Adv. Phys.* **57**, 457 (2008).
 - [6] A. Ruiz, D. Alonso, M. B. Plenio, and A. del Campo, Tuning heat transport in trapped-ion chains across a structural phase transition, *Phys. Rev. B* **89**, 214305 (2014).
 - [7] C. Monroe, W. C. Campbell, L.-M. Duan, Z.-X. Gong, A. V. Gorshkov, P. W. Hess, R. Islam, K. Kim, N. M. Linke, G. Pagano, P. Richerme, C. Senko, and N. Y. Yao, Programmable quantum simulations of spin systems with trapped ions, *Rev. Mod. Phys.* **93**, 025001 (2021).
 - [8] P. Wang, C.-Y. Luan, M. Qiao, M. Um, J. Zhang, Y. Wang, X. Yuan, M. Gu, J. Zhang, and K. Kim, Single ion qubit with estimated coherence time exceeding one hour, *Nat. Commun.* **12**, 233 (2021).
 - [9] D. Kielpinski, C. Monroe, and D. J. Wineland, Architecture for a large-scale ion-trap quantum computer, *Nature (London)* **417**, 709 (2002).
 - [10] D. Leibfried, R. Blatt, C. Monroe, and D. Wineland, Quantum dynamics of single trapped ions, *Rev. Mod. Phys.* **75**, 281 (2003).
 - [11] E. Wigner, On the interaction of electrons in metals, *Phys. Rev.* **46**, 1002 (1934).
 - [12] J. Sólyom, Wigner crystals: New realizations of an old idea, *EPJ Web Conf.* **78**, 01009 (2014).
 - [13] J. P. Schiffer, Phase Transitions in Anisotropically Confined Ionic Crystals, *Phys. Rev. Lett.* **70**, 818 (1993).
 - [14] D. H. E. Dubin, Theory of Structural Phase Transitions in a Trapped Coulomb Crystal, *Phys. Rev. Lett.* **71**, 2753 (1993).
 - [15] D. G. Enzer, M. M. Schauer, J. J. Gomez, M. S. Gulley, M. H. Holzscheiter, P. G. Kwiat, S. K. Lamoreaux, C. G. Peterson, V. D. Sandberg, D. Tupa, A. G. White, R. J. Hughes, and D. F. V. James, Observation of Power-Law Scaling for Phase Transitions in Linear Trapped Ion Crystals, *Phys. Rev. Lett.* **85**, 2466 (2000).
 - [16] N. Kjærgaard and M. Drewsen, Observation of a Structural Transition for Coulomb Crystals in a Linear Paul Trap, *Phys. Rev. Lett.* **91**, 095002 (2003).
 - [17] G. Piacente, I. V. Schweigert, J. J. Betouras, and F. M. Peeters, Generic properties of a quasi-one-dimensional classical Wigner crystal, *Phys. Rev. B* **69**, 045324 (2004).
 - [18] S. Fishman, G. De Chiara, T. Calarco, and G. Morigi, Structural phase transitions in low-dimensional ion crystals, *Phys. Rev. B* **77**, 064111 (2008).
 - [19] Z.-X. Gong, G.-D. Lin, and L.-M. Duan, Temperature-Driven Structural Phase Transition for Trapped Ions and a Proposal for Its Experimental Detection, *Phys. Rev. Lett.* **105**, 265703 (2010).
 - [20] L. Yan, W. Wan, L. Chen, F. Zhou, S. Gong, X. Tong, and M. Feng, Exploring structural phase transitions of ion crystals, *Sci. Rep.* **6**, 21547 (2016).
 - [21] D. Podolsky, E. Shimshoni, G. Morigi, and S. Fishman, Buckling Transitions and Clock Order of Two-Dimensional Coulomb Crystals, *Phys. Rev. X* **6**, 031025 (2016).
 - [22] A. Benassi, A. Vanossi, and E. Tosatti, Nanofriction in cold ion traps, *Nat. Commun.* **2**, 236 (2011).
 - [23] A. Bylinskii, D. Gangloff, and V. Vuletić, Tuning friction atom-by-atom in an ion-crystal simulator, *Science* **348**, 1115 (2015).
 - [24] J. Kiethe, R. Nigmatullin, D. Kalincev, T. Schmirander, and T. Mehlstäubler, Probing nanofriction and Aubry-type signatures in a finite self-organized system, *Nat. Commun.* **8**, 15364 (2017).
 - [25] G.-D. Lin and L. Duan, Equilibration and temperature distribution in a driven ion chain, *New J. Phys.* **13**, 075015 (2011).

- [26] A. Bermudez, M. Bruderer, and M. B. Plenio, Controlling and Measuring Quantum Transport of Heat in Trapped-Ion Crystals, *Phys. Rev. Lett.* **111**, 040601 (2013).
- [27] N. Freitas, E. A. Martinez, and J. P. Paz, Heat transport through ion crystals, *Phys. Scr.* **91**, 013007 (2016).
- [28] L. Timm, H. Weimer, L. Santos, and T. E. Mehlstäubler, Energy localization in an atomic chain with a topological soliton, *Phys. Rev. Research* **2**, 033198 (2020).
- [29] A. Abdelrahman, O. Khosravani, M. Gessner, A. Buchleitner, H.-P. Breuer, D. Gorman, R. Masuda, T. Pruttivarasin, M. Ramm, P. Schindler *et al.*, Local probe of single phonon dynamics in warm ion crystals, *Nat. Commun.* **8**, 15712 (2017).
- [30] M. Tamura, T. Mukaiyama, and K. Toyoda, Quantum Walks of a Phonon in Trapped Ions, *Phys. Rev. Lett.* **124**, 200501 (2020).
- [31] M. Ramm, T. Pruttivarasin, and H. Häffner, Energy transport in trapped ion chains, *New J. Phys.* **16**, 063062 (2014).
- [32] G.-D. Lin and L.-M. Duan, Sympathetic cooling in a large ion crystal, *Quantum Inf. Process.* **15**, 5299 (2016).
- [33] K. Sosnova, A. Carter, and C. Monroe, Character of motional modes for entanglement and sympathetic cooling of mixed-species trapped-ion chains, *Phys. Rev. A* **103**, 012610 (2021).
- [34] Z.-C. Mao, Y.-Z. Xu, Q.-X. Mei, W.-D. Zhao, Y. Jiang, Y. Wang, X.-Y. Chang, L. He, L. Yao, Z.-C. Zhou, Y.-K. Wu, and L.-M. Duan, Experimental Realization of Multi-ion Sympathetic Cooling on a Trapped Ion Crystal, *Phys. Rev. Lett.* **127**, 143201 (2021).
- [35] R. Blatt and D. Wineland, Entangled states of trapped atomic ions, *Nature (London)* **453**, 1008 (2008).
- [36] C. Monroe and J. Kim, Scaling the ion trap quantum processor, *Science* **339**, 1164 (2013).
- [37] V. Giovannetti, S. Lloyd, and L. Maccone, Quantum-enhanced measurements: Beating the standard quantum limit, *Science* **306**, 1330 (2004).
- [38] K. A. Gilmore, M. Affolter, R. J. Lewis-Swan, D. Barberena, E. Jordan, A. M. Rey, and J. J. Bollinger, Quantum-enhanced sensing of displacements and electric fields with two-dimensional trapped-ion crystals, *Science* **373**, 673 (2021).
- [39] Y.-Z. Xu, W.-D. Zhao, Y.-H. Hou, Q.-X. Mei, J.-Y. Ma, J. Wang, L. He, Z.-C. Zhou, Y.-K. Wu, and L.-M. Duan, Controlled melting of a Wigner ion crystal with atomic resolution, *Phys. Rev. A* **102**, 063121 (2020).
- [40] K. A. Landsman, Y. Wu, P. H. Leung, D. Zhu, N. M. Linke, K. R. Brown, L. Duan, and C. Monroe, Two-qubit entangling gates within arbitrarily long chains of trapped ions, *Phys. Rev. A* **100**, 022332 (2019).
- [41] B. Srivathsan, M. Fischer, L. Alber, M. Weber, M. Sondermann, and G. Leuchs, Measuring the temperature and heating rate of a single ion by imaging, *New J. Phys.* **21**, 113014 (2019).
- [42] M. D’Onofrio, Y. Xie, A. J. Rasmusson, E. Wolanski, J. Cui, and P. Richerme, Radial Two-Dimensional Ion Crystals in a Linear Paul Trap, *Phys. Rev. Lett.* **127**, 020503 (2021).